

## Chapter 3

# Atmospheric Radiative Transfer Model

### 3.1 Overview

This chapter deals with the development of a radiative transfer model of the atmosphere of the earth in IDL<sup>®</sup>. Section 3.2: FASCODE Radiative Transfer Model describes the FASCODE radiative transfer model and discusses its strengths and weaknesses. Section 3.3: Atmospheric Modelling describes the methods used to calculate pressure, temperature, and density for the individual layers of the atmospheric model. Section 3.4: Line Shape Modelling describes the process of calculating the Voigt line shape, the water vapour line shape, and water vapour continuum. Section 3.5: University of Lethbridge Transmittance and Radiance Model discusses the line-by-line, layer-by-layer algorithm of the model and presents results of the modelling program, including a comparison with the FASCODE

model.

## 3.2 FASCODE Radiative Transfer Model

Beginning in the 1970's, there was an effort to develop a fast radiative transfer model for the purposes of analyzing the spectral characteristics of the atmosphere. This model is known as the Fast Atmospheric Signature Code or by its acronym, FASCODE [9]. The FASCODE radiative transfer model has its origins in the atmospheric research division of the United States Air Force. Its original purpose was to allow for the identification of the spectral signatures of the exhaust emissions of enemy weapon systems.

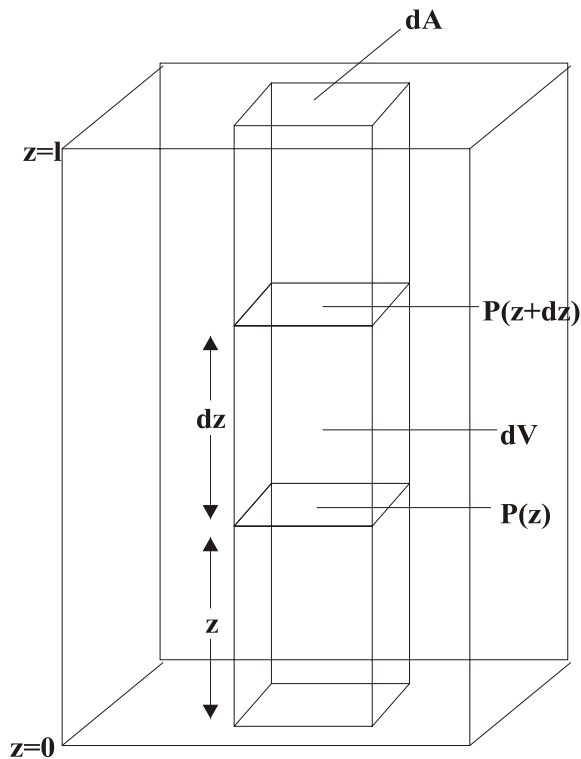
FASCODE is a well known radiative transfer model of the atmosphere which finds frequent use by researchers. The model has some flexibility with six different built-in atmospheric profiles of pressure, temperature, and molecular densities as a function of altitude. These atmospheric profiles are specific to certain geographic regions such as the tropics or mid-latitudes. The model also allows for a user defined atmospheric profile. FASCODE is also flexible in terms of the atmospheric path travelled by the radiation (e.g. ground to sky, sky to ground, sky to sky); the path can start and end at any altitude along any zenith angle.

While FASCODE is a general purpose tool for radiative transfer modelling, it has two principal limitations that reduce its effectiveness for modelling the transmission spectrum of the atmosphere above Mauna Kea. The first limitation is that the program is general, rather than location-specific, because it was developed to model the atmosphere in any geographic area of the world. In particular, as shown in § 3.3.4, the atmosphere above

Mauna Kea is significantly different than the tropical atmospheric profile in the FASCODE database.

The second principal limitation of FASCODE is that it was developed with the goal of simulating essentially an infinite number of observing geometries. As a result of this flexibility, FASCODE is well over 1000 pages of user-unfriendly Fortran code. The main program itself has 71,000 lines of code and is 700 pages long. Because of its size, it is not easy to make sensible changes to FASCODE and understand their impact throughout the program.

FASCODE has proven useful as a radiative transfer model; however, it is too general to model accurately the atmosphere above Mauna Kea. These limitations created the impetus for the development of a simpler radiative transfer model in a modern computer language. The goals of developing a new model were to allow for a *user-definable model atmosphere* and to produce a well documented, user-friendly code. The development of the radiative transfer model, which was written in the fourth generation language Interactive Data Language (IDL<sup>®</sup>) [10], found in many active research environments, will be detailed in the following sections of this chapter.



**Definition of pressure differential**

$$dP = P(z+dz) - P(z)$$

**Buoyant force on volume element dV**

$$F_B = [P(z) - P(z+dz)] dA \\ = - dP dA$$

**Gravitational force on volume element dV**

$$F_g = - mg = - \rho(z) dz dA g$$

**Equilibrium condition**

$F_B + F_g = 0$  yields the hydrostatic equation:  
 $dP = - g \rho(z) dz$

Figure 3.1: The hydrostatic equation describes the gravitationally induced vertical density profile  $\rho = \rho(z)$  where  $z$  is the altitude measured from ground level.

### 3.3 Atmospheric Modelling

#### 3.3.1 Pressure, Density, and the Hydrostatic Equation

The atmosphere is bound to the earth by the gravitational field such that its pressure and density both decrease with increasing altitude. In the following analysis the atmosphere is assumed to be in static equilibrium. Under this assumption, the pressure,  $p$ , of the atmosphere at an altitude  $z$  can be found from the hydrostatic equation [11]

$$dp = -g\rho dz \tag{3.1}$$

where

$$g(z) = \frac{GM_E}{(R_E + z)^2} \quad \text{m} \cdot \text{s}^{-2} \quad (3.2)$$

is the acceleration due to gravity at altitude  $z$ . In equation 3.2,  $G = 6.673 \times 10^{-11} \text{ m}^3 \cdot \text{kg}^{-1} \cdot \text{s}^{-2}$  is the Newtonian constant of gravitation,  $M_E = 5.974 \times 10^{24} \text{ kg}$  is the mass of the earth, and  $R_E = 6.378 \times 10^6 \text{ m}$  is the radius of the earth. At sea level,  $g(0) = 9.800 \text{ m} \cdot \text{s}^{-2}$ . As one moves upwards in the atmosphere, the value of  $g$  declines. At the summit of Mauna Kea, at an altitude of 4092 m,  $g(4092) = 9.787 \text{ m} \cdot \text{s}^{-2}$ . In the upper-most part of the atmosphere, at an altitude of 50 km, the acceleration due to gravity is  $g(50 \text{ km}) = 9.648 \text{ m} \cdot \text{s}^{-2}$ .

From the equation of state for a perfect gas, the density,  $\rho$ , of the atmosphere is

$$\rho = \frac{M_r p}{RT} \quad \text{kg} \cdot \text{m}^{-3} \quad (3.3)$$

where  $M_r$  is the molar mass of the gas in  $\text{kg} \cdot \text{mol}^{-1}$ ,  $p$  is the pressure in Pa,  $R = 8.314 \text{ J} \cdot \text{mol}^{-1} \cdot \text{K}^{-1}$  is the universal gas constant, and  $T$  is the temperature in Kelvin.

Expressed in terms of density, equation 3.1 becomes

$$\frac{dp}{p} = \frac{-dz}{H} \quad (3.4)$$

where  $H = \frac{RT}{M_r g}$  is known as the *scale height* in m. This scale height represents the increase in altitude corresponding to a decrease in pressure by a factor of  $e$ , and is itself a function of altitude since  $M_r$ ,  $g$ , and  $T$  are all altitude dependent. The variation of temperature,  $T$ , with altitude is discussed in § 3.3.2.

Equation 3.4 can be integrated to give the pressure at an altitude of  $z$  as

$$p(z) = p_0 e^{\int_{z_0}^z \frac{dz}{H(z)}} \quad \text{mbar} \quad (3.5)$$

where  $p_0$  is the pressure at a reference altitude. Since the density of the gas is directly proportional to the pressure, it can be calculated using the formula

$$\rho(z) = \rho_0 e^{\int_{z_0}^z \frac{dz}{H(z)}} \quad \text{kg} \cdot \text{m}^{-3} \quad (3.6)$$

where  $\rho_0$  is the density at the reference altitude of  $z_0$ .

Finally, *number density*,  $n(z)$  is related to pressure by the equation

$$n(z) = \frac{p(z)}{k_B T(z)} \quad \text{molecules} \cdot \text{m}^{-3} \quad (3.7)$$

where  $k_B = 1.381 \times 10^{-23} \text{ J} \cdot \text{K}^{-1}$  is the Boltzmann constant, and  $T(z)$  is the temperature in K.

Using equations 3.5 and 3.7, it is straight forward to calculate the pressure and molecular number density at any altitude in the atmosphere. However, in order to calculate the overall transmission and emission, it is necessary to divide the atmosphere into layers such that several layers span each scale-height-sized section in the atmosphere. Furthermore, the atmosphere in each layer is treated as being homogeneous throughout the layer by finding *equivalent values* for each of the atmospheric parameters.

Since pressure and number density do not vary linearly through the layer, a simple average of the layer boundary values of these quantities is, in general, not adequate to describe the overall conditions of the layer. An equivalent pressure can be found for each

layer by calculating a *weighted average* of the pressure throughout the layer. The weighted average of pressure in a layer is found by [11]

$$\bar{P} = \frac{\int p \, du}{\int du} \quad \text{mbar} \quad (3.8)$$

where  $du = n(z) \, dz$ . This averaging procedure is known as the *Curtis-Godson approximation*.

In essence, equation 3.8 accounts for the fact that pressure is not linearly dependent on altitude. From the equivalent pressure, an equivalent density,  $\bar{\rho}$ , can be calculated from equation 3.3 and an equivalent number density,  $\bar{n}$ , can be calculated from equation 3.7 using the average temperature from equation 3.19 in the next section. The equivalent layer values of pressure, temperature, and density define the *physical characteristics* of the layer and are the inputs to the radiative transfer program.

### 3.3.2 Atmospheric Temperature Profile

If an element of gas moves adiabatically in the atmosphere, the first law of thermodynamics requires that

$$c_v \, dT = -p \, dV \quad (3.9)$$

where  $c_v$  is the specific heat capacity of the atmosphere at a constant volume in  $\text{J}\cdot\text{kg}^{-1}\cdot\text{K}^{-1}$ .

If  $V$  is the *specific volume* containing a gram of molecules, then the ideal gas law gives

$$dV = \frac{N_0 k_B}{p} \, dT - \frac{N_0 k_B T}{p^2} \, dp \quad (3.10)$$

where  $N_0 = 1/M$  and  $M$  is the molecular mass of the atmosphere. Since  $c_p = c_v + N_0 k_B$ , equation 3.10 can be rewritten as

$$c_p dT = \frac{N_0 k_B T}{p} dp = V dp = \frac{1}{\rho} dp \quad (3.11)$$

Using the hydrostatic equation (equation 3.1), a relation between height and atmospheric temperature can be defined [11]

$$\frac{dT}{dz} = \frac{-g}{c_p} = -\Gamma_d \quad \text{K} \cdot \text{m}^{-1} \quad (3.12)$$

where  $c_p$  is the specific heat capacity of the atmosphere at constant pressure in  $\text{J} \cdot \text{kg}^{-1} \cdot \text{K}^{-1}$  and  $\Gamma_d$  is known as the *adiabatic lapse rate*. For dry air,  $c_p = 1005 \text{ J} \cdot \text{kg}^{-1} \cdot \text{K}^{-1}$ , which gives an adiabatic lapse rate of  $\Gamma_d \simeq 10 \text{ K} \cdot \text{km}^{-1}$ . This means that for every increase in altitude of 1 km, the temperature of the atmosphere drops by 10 K.

Equation 3.12 excludes water vapour from the atmosphere. Water can exist as solid, liquid, or gas in the atmosphere. When the presence of water in the atmosphere is taken into account, a *wet adiabatic lapse rate* is given by [21]

$$\frac{dT}{dz} = \frac{-g/c_p}{1 + (L/c_p)(dw_s/dT)} = -\Gamma \quad \text{K} \cdot \text{m}^{-1} \quad (3.13)$$

where  $w_s$  is the mass of saturated water per mass of air and  $L$  is the latent heat of vaporization. The wet lapse rate is about half the dry lapse rate, around  $5 \text{ K} \cdot \text{km}^{-1}$ .

The sizable temperature gradient in the atmosphere leads to convection of both dry air and wet air, resulting in a mix of temperature gradients. Due to this convective mixing, the troposphere has an average lapse rate of  $6.5 \text{ K} \cdot \text{km}^{-1}$  [21]. Recent measurements by balloon-borne radiosondes launched from Hilo, Hawaii have shown that the atmosphere

above Mauna Kea has an average lapse rate of about  $5.6 \text{ K km}^{-1}$  [22]. This was confirmed by an analysis of 80 radiosondes launched from Hilo airport in 1999. The radiosonde data were averaged together and an IDL program was written to find the lapse rate of the average pressure-temperature curve (shown as the black line in figure 3.2). The average lapse rate for the atmosphere above Mauna Kea was determined to be  $5.7 \pm 0.9 \text{ K}\cdot\text{km}^{-1}$ . The theoretical pressure-temperature curve with a lapse rate of  $5.7 \text{ K km}^{-1}$  used by ULTRAM is shown in the figure as the green line, while the error is represented by the red curves. The pressure-temperature curve from the FASCODE tropical atmosphere profile is shown as a blue line in figure 3.2. The pressure-temperature curve used by ULTRAM is much closer to the average of the radiosonde data than the FASCODE curve.

In the lower atmosphere, the temperature decreases with increasing altitude. In the upper atmosphere, however, it is important to consider a number of reactions involving oxygen, known as the *Chapman reactions* [21]. Molecular oxygen is photodissociated by absorption in the Herzberg continuum according to



The atomic oxygen then bonds to  $\text{O}_2$  in the presence of an unspecified third body, M, to form ozone



Both O and  $\text{O}_3$  are destroyed by



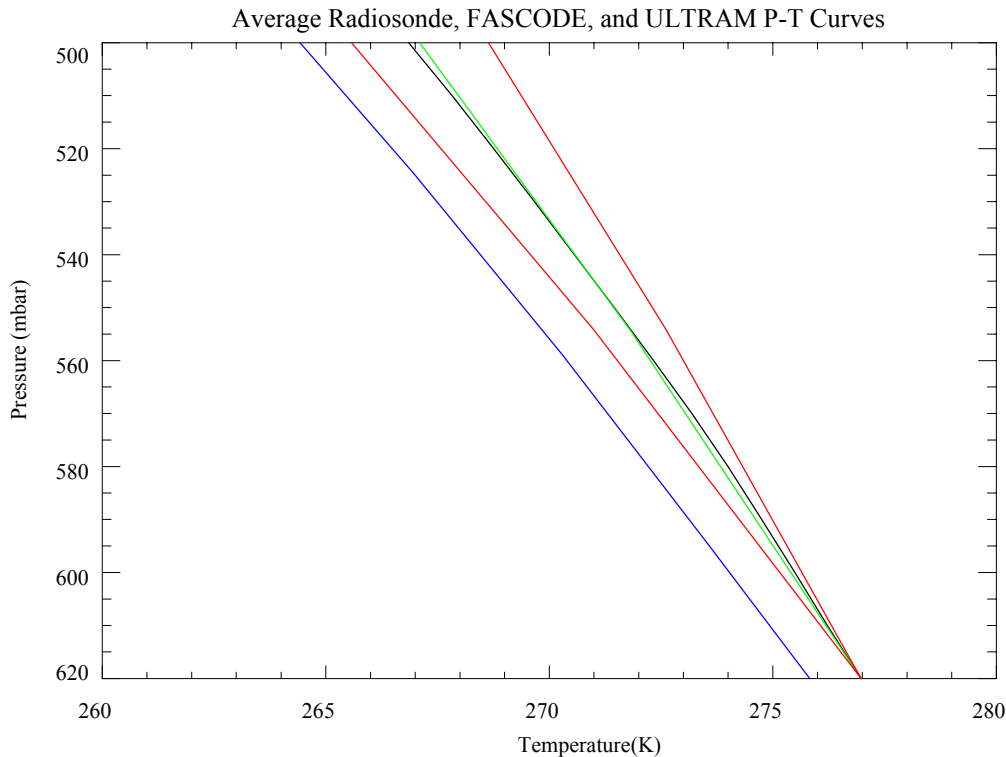


Figure 3.2: A comparison of the average of radiosonde data above Mauna Kea (black) with the pressure-temperature curves from the FASCODE tropical atmosphere profile (blue) and ULTRAM (green) calculated with a lapse rate of  $5.7 \pm 0.9$  K/km. The error in the ULTRAM lapse rate is represented by the pair of red lines.

and  $O_3$  is converted back to  $O$  by, among other processes



resulting in a temperature increase. This increased temperature creates an *inversion layer*, effectively decoupling the lower atmosphere (*troposphere*) from the *stratosphere*. The highest concentrations of ozone are found in the stratosphere (10 - 50 km) with peak ozone levels at an altitude of  $\sim 25$  km in the tropics. The principle source of heating in the ozone layer is due to the ozone dissociation as shown in equation 3.17. Since the increase in temperature is non-linear and dependent on latitude (as is the concentration of ozone),

modelling the temperature is difficult at these altitudes. In this thesis, the temperature of the atmosphere at altitudes where ozone heating is significant has been taken from the tabulated temperature data in the tropical atmosphere model in FASCODE.

In ULTRAM, the temperature at a layer boundary at altitude  $z$  is given by

$$T(z) = T_0 - \Gamma \cdot z \quad \text{K} \quad (3.18)$$

where  $T_0$  is the base temperature and  $\Gamma$  is the temperature lapse rate of  $5.7 \text{ K}\cdot\text{km}^{-1}$ . Above an altitude of 12 km, heating due to the absorption of ultraviolet radiation by ozone leads to an increase in temperature and, as mentioned above, temperature data for this region have been taken from the tropical atmospheric model in FASCODE.

Other computations in the model are simplified if the temperature is constant through a layer. Since the temperature varies almost linearly with altitude, the equivalent temperature of a layer is found by taking the average of the temperatures at the layer boundaries

$$\bar{T} = \frac{T(z) + T(z + dz)}{2} \quad \text{K} \quad (3.19)$$

This is the equivalent temperature of the layer mentioned in § 3.3.1.

### 3.3.3 Molecular Constituents in the Atmosphere

This thesis is primarily concerned with two spectral regions: the submillimeter region ( $5 \text{ cm}^{-1} - 35 \text{ cm}^{-1}$ ) and the mid-infrared region ( $475 \text{ cm}^{-1} - 575 \text{ cm}^{-1}$ ). The primary absorbing molecular species in the submillimeter region are water vapour, molecular

oxygen, and ozone. In the mid-infrared region, the primary absorbers are water vapour, carbon dioxide, and nitrous oxide (N<sub>2</sub>O).

ULTRAM adopted the FASCODE formalism in which tabulated values of *mixing ratios* are stored in the atmospheric model database. The volume mixing ratio is defined as the ratio of the number of molecules of a certain species,  $N_g$ , to the total number molecules,  $N_T$

$$r = \frac{N_g}{N_T} \quad (3.20)$$

The mixing ratio for a given absorber varies with height, so the mixing ratios at the boundaries of a layer have been determined through spline interpolation. By choosing sufficiently thin layers (i.e. with several per scale height), an equivalent mixing ratio, equal to the average of the mixing ratios at the layer boundaries, can be assigned to each layer

$$\bar{r} = \frac{r(z) + r(z + dz)}{2} \quad (3.21)$$

This mixing ratio is used to calculate the average number density of molecules of a certain species,  $\bar{n}_g$ , in a layer by

$$\bar{n}_g = \bar{r}\bar{n} \quad \text{molecules} \cdot \text{cm}^{-3} \quad (3.22)$$

where  $\bar{n}$  is the average number density of all molecules in the layer. A column abundance of a certain species,  $du_g$ , for the layer can then be calculated, giving

$$du_g = \bar{n}_g dz \quad \text{molecules} \cdot \text{cm}^{-2} \quad (3.23)$$

ULTRAM determines the column abundances of oxygen, carbon dioxide, and ozone using the tabulated mixing ratios from the FASCODE tropical atmospheric model. First,

the mixing ratios at the layer boundaries are found by spline interpolation of the tabulated data. Average mixing ratios for each molecule are determined using equation 3.21 and these are used to determine average molecular number densities with equation 3.22. Finally, molecular column abundances for each molecule are determined from equation 3.23.

Water vapour is a minor constituent of the troposphere with concentrations often measured in parts per million. However, it is a major contributor in both spectral regions of interest. The distribution of water vapour is not well known; unlike the other gases discussed, water vapour is highly polar and can form strong intermolecular hydrogen bonds. These intermolecular hydrogen bonds often lead to the clustering of the water vapour molecules, forming polymers and, ultimately, raindrops. One might expect that water vapour should be distributed exponentially with a scale height found by

$$H_{H_2O} = \frac{RT}{gM_{H_2O}} \quad \text{km} \quad (3.24)$$

where  $M_{H_2O} = 18.02 \text{ g}\cdot\text{mol}^{-1}$  is the molar mass of water. At the summit of Mauna Kea, where temperatures are typically near 270 K and  $g = 9.787 \text{ m}\cdot\text{s}^{-2}$ , equation 3.24 gives a scale height for water vapour of  $H_{H_2O} = 12.73 \text{ km}$ . However, this scale height is much larger than the scale height of water vapour observed in the real atmosphere,  $H_{H_2O} \simeq 2 \text{ km}$ . This reduction in the scale height is due to the fact that water vapour precipitates out of the atmosphere at relatively high temperatures compared to other gases.

In this approximation, the number density of water vapour at height  $z$  can be expressed as

$$n_{H_2O}(z) = n_{H_2O,0} e^{-\frac{z}{H_{H_2O}}} \quad \text{molecules} \cdot \text{cm}^{-3} \quad (3.25)$$

where  $n_{H_2O,0}$  is the number density of water vapour at the base altitude and  $H_{H_2O} = 2$  km. Following the previous analysis, a Curtis-Godson approximation can be used to give an average number density of water vapour in a layer.

Another measure of the amount of water vapour in the atmosphere is known as the *precipitable water vapour* (pww). If all of the water vapour in a column of atmosphere above a unit area was condensed into a container, then the precipitable water vapour is the depth of the condensed water in millimeters (mm).

Another convenient measure of the amount of a species in the atmosphere is known as *partial pressure*. The partial pressure of a species is the pressure exerted only by molecules of the species of interest. The partial pressure,  $e_g$ , is related to the volume mixing ratio by

$$e_g(z) = r(z) p(z) \quad \text{mbar} \quad (3.26)$$

where  $p(z)$  is the pressure at the same altitude as the mixing ratio,  $r(z)$ . An average partial pressure can be computed by simply replacing the values in equation 3.26 with their respective averages.

### 3.3.4 Comparison of ULTRAM Atmosphere to Hilo Radiosondes

Figure 3.3 shows the average pressure-temperature curve determined from 80 radiosondes launched from Hilo airport, located nearby Mauna Kea. The black curve in the figure is the average pressure-temperature curve, while the red curves represent a  $1\sigma$  error. The green curve in the figure shows the pressure-temperature curve from the atmospheric

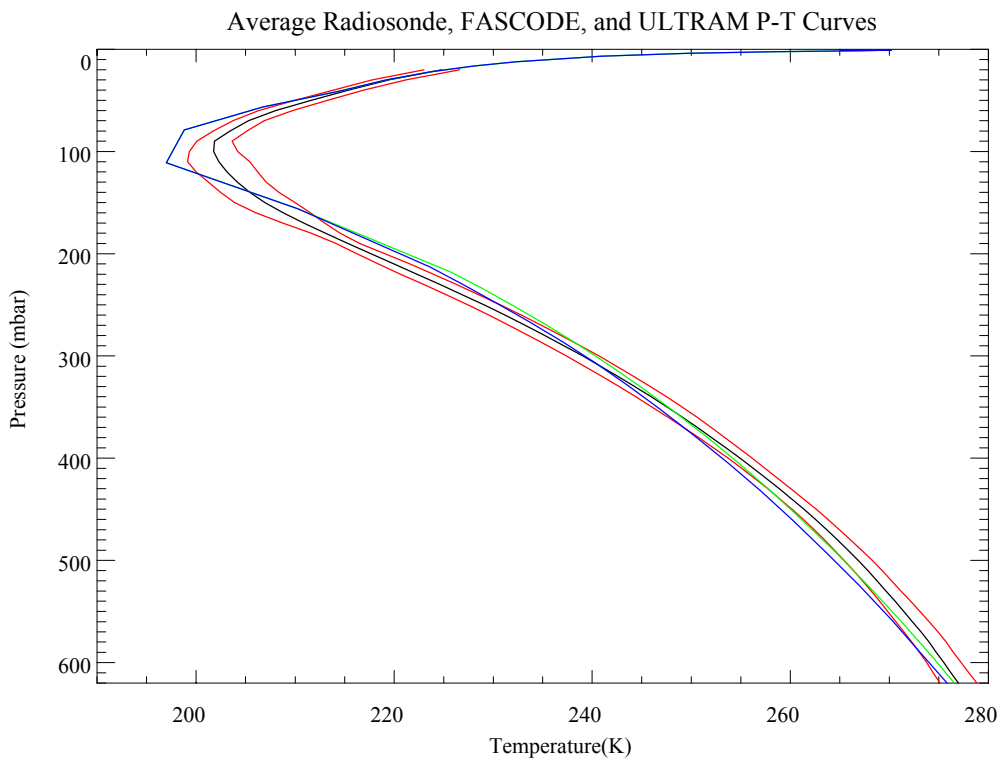


Figure 3.3: A comparison of the average of the radiosonde data (black) with the pressure-temperature curve from the FASCODE tropical atmosphere model (blue) and the pressure-temperature curve of ULTRAM (green). The standard deviation of the radiosonde data is shown in red.

model of ULTRAM. This curve was determined from equations 3.5 and 3.18 using a pressure of 625 mbar, an air temperature of 273 K, and a lapse rate of  $5.7 \text{ K km}^{-1}$ , typical conditions at the summit of Mauna Kea.

The theoretical pressure-temperature curve fits well with the average of the radiosonde data. From this, it can be seen that the atmospheric model used by ULTRAM is in close agreement with the measured profile of the atmosphere above Mauna Kea.

## 3.4 Radiative Transfer Model

### 3.4.1 Spectral Line Shape in the Real Atmosphere

In § 2.4.2, several broadening mechanisms and their associated line shapes were discussed. Both the Lorentz and Doppler line shapes must be considered when modelling spectral lines in the atmosphere. The Lorentz line shape is dominant at the lower altitudes where the pressure is high and molecular collisions occur more frequently. The Doppler line shape becomes dominant in the upper atmosphere where the pressure is lower, reducing the Lorentzian contribution to line width.

In the mid-altitude atmosphere, where neither Lorentz nor Doppler are dominant, the Voigt line shape, shown in figure 3.4, is used. The Voigt line shape, a convolution of the Lorentz and Doppler shapes, resembles the broad Lorentz shape at high pressures. At low pressures the Voigt shape closely resembles the thinner Doppler shape. Between the Doppler and Lorentz regimes, the Voigt shape is a mix of both line shapes, with a strong central component similar to the Doppler shape and broad wings reflecting the Lorentz component. The equation for the Voigt line shape is [23]

$$f(\sigma - \sigma_0) = \frac{a}{\gamma_D \sqrt{\pi^3}} \int_{-\infty}^{\infty} \frac{e^{-y^2}}{a^2 + (q - y)^2} dy \quad \text{cm} \quad (3.27)$$

where

$$a = \frac{\gamma_L}{\gamma_D} \quad (3.28)$$

and

$$q = \frac{\sigma - \sigma_0}{\gamma_D} \quad (3.29)$$

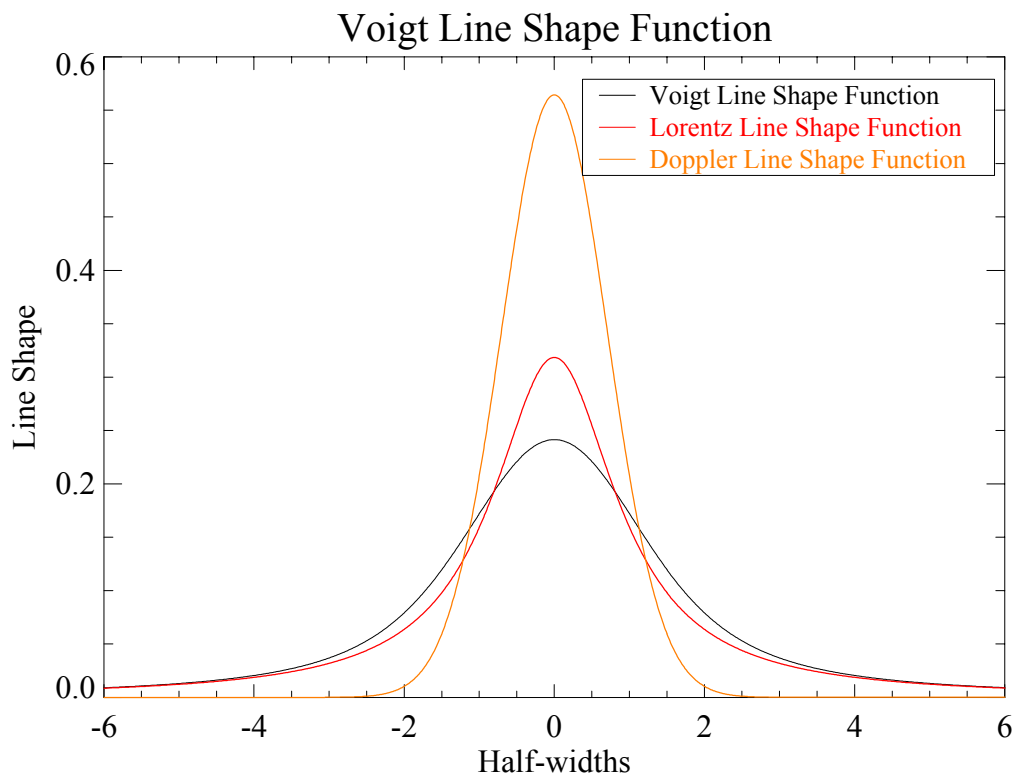


Figure 3.4: A comparison of the Voigt line shape function (black), the Doppler line shape function (orange), and the Lorentz line shape function (red).

In figure 3.4, the Voigt line shape function is calculated using Doppler and Lorentz line shapes of the same half-width. All three of the line shapes in the figure were normalized to unit area so that they all represent the same amount of absorption.

The Voigt line shape is the best representation of the actual line shape for most spectral lines in the atmosphere. It accurately reproduces the Doppler-dominated shape of ozone lines as well as the broad, Lorentz-dominated line shape of water vapour lines. It would be challenging to develop a numerical method of integration for this function. Fortunately, IDL<sup>®</sup> has a built in routine to calculate the value of the Voigt function at any distance from the line center and this has been used to calculate line shapes in the present

model.

One problem with the Voigt line profile is that it does not accurately model the behavior of water vapour lines [24]. The special line shape used to model water vapour is discussed in the next section.

### 3.4.2 Water Vapour Spectral Line Shape and Continuum

The shape of water vapour lines is radically different from that of any other species. Since water vapour is only found in the lower reaches of the atmosphere, its line shape somewhat resembles the pressure broadened Lorentzian profile. However, the line wings are significantly stronger than any other species. In fact, these line wings often extend beyond  $25 \text{ cm}^{-1}$  from the line center.

The strong line wings of water vapour are thought to be due to the strong polar nature of this molecule [24] which allows it to form strong associations with other water molecules in the atmosphere. Due to their polar nature, water vapour molecules experience prolonged interactions during collisions. The Lorentz line shape is a good representation for those molecules where collisions are instantaneous but it cannot accurately describe the line shape of the spectral lines of water vapour.

Following the work of Clough, Kneizys, and Davies (CKD) [24], the water vapour line shape is expressed with an absorption coefficient of

$$k_{H_2O} = k_{line} + k_{cont} \quad (3.30)$$

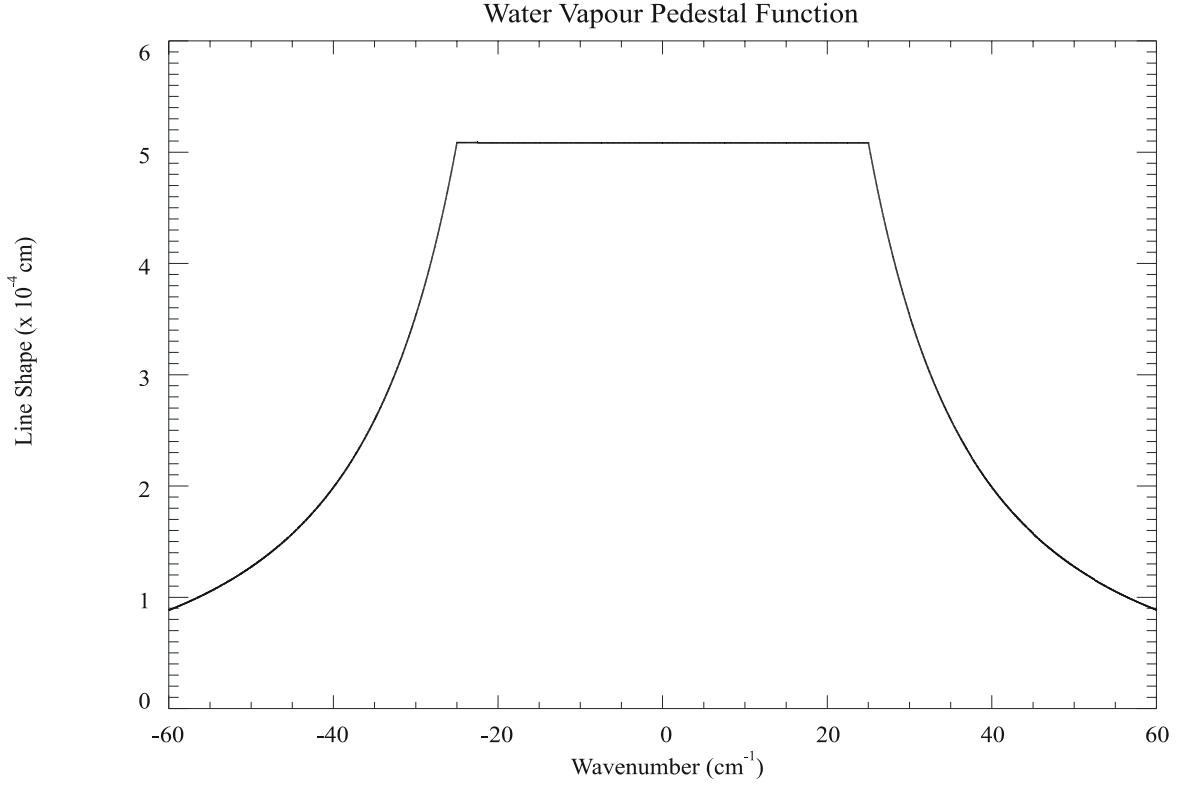


Figure 3.5: A plot of the pedestal function subtracted from the line shape function of water vapour.

where  $k_{line}$  is the absorption coefficient for line shape and  $k_{cont}$  is an empirical correction term known as the *water vapour continuum*. The CKD continuum coefficients used in this thesis were obtained from version 3 of the FASCODE program [25].

The theoretical portion of the water vapour line shape,  $f_{line}$ , is given by the Voigt line shape with a pedestal-shaped function subtracted from it. The pedestal shape function is given by [24]

$$f_{pedestal} = \frac{1}{\pi} \frac{\gamma_L}{25^2 + \gamma_L^2} \quad \text{cm} \quad (3.31)$$

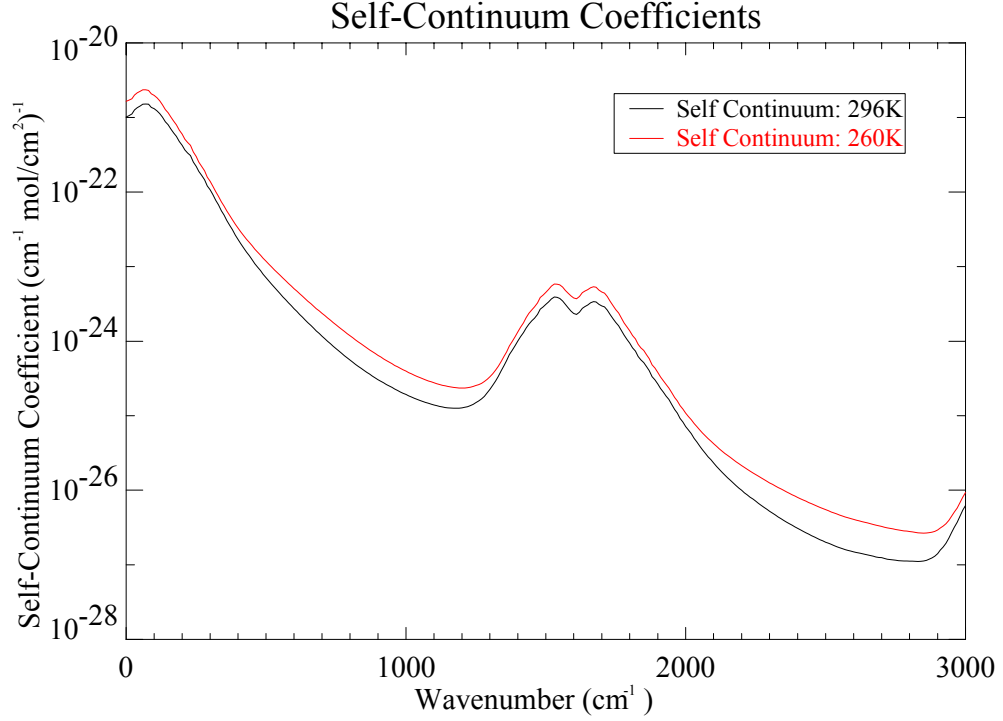


Figure 3.6: A plot of the CKD self-continuum coefficients.

for  $|\sigma \mp \sigma_0| \leq 25 \text{ cm}^{-1}$  and

$$f_{pedestal} = \frac{1}{\pi} \frac{\gamma_L}{(\sigma \mp \sigma_0)^2 + \gamma_L^2} \quad \text{cm} \quad (3.32)$$

for  $|\sigma \mp \sigma_0| \geq 25 \text{ cm}^{-1}$ , where  $\gamma_L$  is the half width of the Lorentz line shape and  $\sigma_0$  is the line center wavenumber. Figure 3.5 shows the pedestal function for the Voigt line shape function defined above.

The subtraction of the pedestal function from the Voigt shape function removes the line wings from the water line. If the contributions of all real water vapour line wings are summed together, the result is a smoothly varying continuum curve. Since water

vapour lines are broadened by collisions with other water vapour molecules and foreign species, the line wings have both a *self-broadened* contribution and a *foreign-broadened* contribution. The contributions are quantified by two sets of coefficients, the self-coefficients shown in figure 3.6 and the foreign-coefficients shown in figure 3.7. Both the self-coefficients and foreign-coefficients are stored in tabular form in the FASCODE program. The self-coefficients are stored for two temperatures, 260 K and 296 K, and must be corrected to the temperature of the layer using the equation [9]

$$C_s = C_s^{296} \left( \frac{C_s^{260}}{C_s^{296}} \right)^{\frac{T-296}{260-296}} \quad (3.33)$$

where  $C_s^{296}$  is the self-coefficient for 296 K,  $C_s^{260}$  is the self-coefficient for 260 K, and  $T$  is the equivalent temperature of the layer. The foreign-coefficients are not affected by temperature and need no correction.

The opacity due to the water vapour continuum is given by [26]

$$k_{cont} = \sigma \tanh \left( \beta \frac{100 \times \sigma}{2} \right) \left[ C_s \left( \frac{e}{p_0} \right) + C_f \left( \frac{p - e}{p_0} \right) \right] \quad (3.34)$$

where  $\beta = \frac{hc}{k_B T}$ ,  $e$  is the partial pressure of water vapour in Pa,  $p$  is the pressure of the atmosphere in Pa, and  $p_0$  is the base pressure of  $1.013 \times 10^5$  Pa.

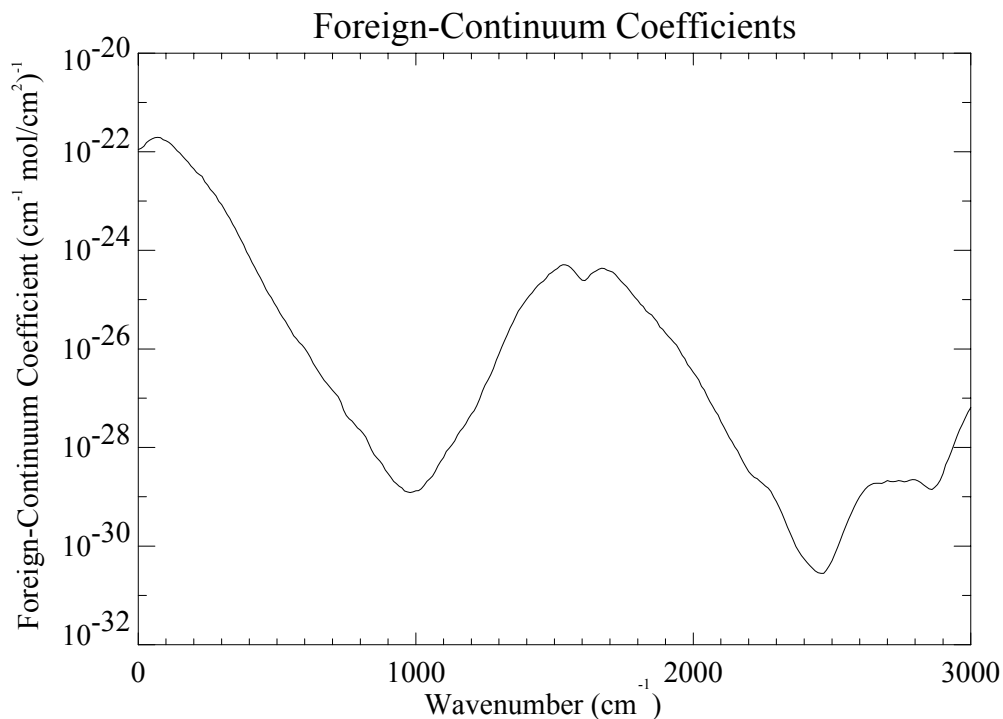


Figure 3.7: A plot of the CKD foreign-continuum coefficients.

## 3.5 University of Lethbridge Transmittance and Radiance Atmospheric Model

### 3.5.1 Model Description

The University of Lethbridge Transmittance and Radiance Atmospheric Model, or ULTRAM, was written in Interactive Data Language 5.4 (IDL 5.4<sup>®</sup>) [10]. IDL<sup>®</sup> was chosen as the development language because of its powerful array processing capabilities.

Most radiative transfer models, such as FASCODE and ULTRAM, are known as

*line-by-line*, *layer-by-layer* radiative transfer models because of the method used. The term ‘line-by-line’ refers to the fact that the contribution to opacity at a specific wavelength by each spectral line must be calculated separately. These contributions can then be summed together using equation 2.29 to give the overall opacity. The ‘layer-by-layer’ term refers to the fact that the model approximates the atmosphere as a series of layers, extending from space to ground. The spectral conditions are calculated for each layer in sequence from space to the ground, tracking the absorption and emission of radiation through the layers.

The IDL<sup>®</sup> array routines are well suited to efficient line-by-line calculations. Most computer languages need to loop through each line to calculate its contribution to opacity at the given wavenumber. This would take a large amount of time since there are thousands of spectral lines contributing to the opacity. IDL<sup>®</sup> can handle the line-by-line calculation using large arrays of line parameters instead of looping through each line individually. This advantage is due to the specially developed array processing routines that set IDL<sup>®</sup> apart from other computer languages.

The main goal in the development of ULTRAM was to provide the user with the flexibility to model radiative transfer under local conditions. The compactness of the IDL<sup>®</sup> code allows users to customize ULTRAM for their own specific purposes while saving them from unpredictable consequences in other parts of the code, as was a danger with FASCODE.

ULTRAM is a user-friendly and flexible program. Users can generate their own model atmospheres using the MAKE\_ATMOSPHERE program, select either the radiance or the transmittance of the atmosphere, uses the CKD continuum coefficients from version

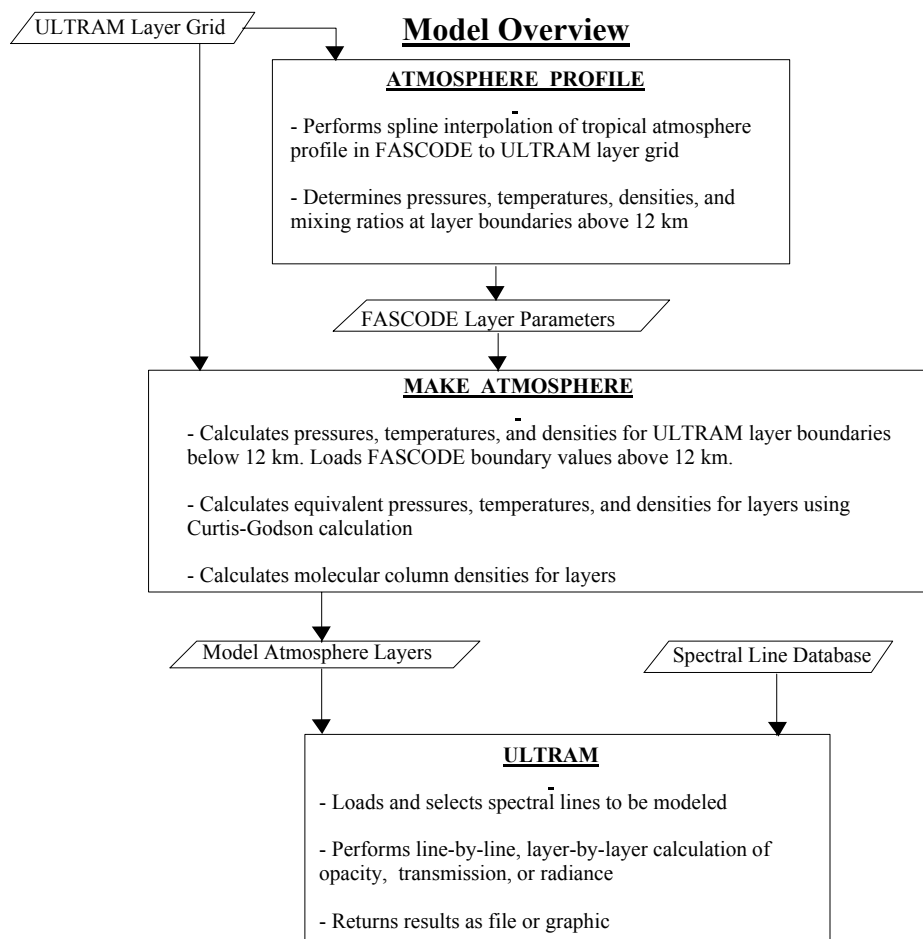


Figure 3.8: Flowchart outlining the general operation of ULTRAM.

3 of the FASCODE program [25] water vapour continuum, or choose not to include the continuum component. Further customizing of features is easily accomplished.

### 3.5.2 Model Algorithm

One of the important inputs to the ULTRAM program are the atmospheric layer boundaries. The default layer boundaries for ULTRAM were defined by iteratively de-

Layer Altitude	Layer Thickness	Number of Layers
4092 - 4500 m	408 m	1
4500 - 12000 m	500 m	15
12 - 30 km	2 km	9
30 - 50 km	4 km	5

Table 3.1: Default ULTRAM layer thicknesses.

creasing the layer thickness from 5 km to 100 m through the entire atmosphere and making comparisons to determine the difference in the spectra produced. The desire for efficiency in the model required that the number of layers be few enough to produce a spectrum in a reasonable time frame ( $\sim 20$  minutes) but be thin enough to allow for an accurate spectrum to be produced. It was found that in the lower atmosphere (4092 m to 12000 m), where water vapour is present with a scale height of  $\sim 2$  km, that layers of 500 m thickness were the optimum size to balance accuracy with efficiency. In the stratosphere, from 12 km to 30 km, layers of 2 km thickness provided the best balance. From 30 to 50 km, layers of 4 km thickness were used. This layering scheme, shown in table 3.1, is the default; however, the user can input whatever layering scheme he or she chooses.

The flowchart in figure 3.8 gives a general outline of the model algorithm. The first step in the modelling program is to perform a spline interpolation of the FASCODE atmospheric parameters to the same layering grid as used by ULTRAM. These parameters will be used to describe the atmosphere above 12 km altitude since the modelling of this region is beyond the scope of this thesis. Next, ULTRAM creates a model atmosphere by calculating pressures, densities, and temperatures for layers below 12 km from the equations in § 3.3 and combining them with the parameters for layers above 12 km from FASCODE. Finally, the model atmosphere file is passed to the main radiative transfer model program

which loads the spectral lines to be used and performs the radiative transfer simulation. Each of these processes is described in more detail in the following paragraphs.

The first step in the modelling process is to create a profile of the various atmospheric parameters ( $P$ ,  $T$ ,  $n$ ,  $n_g$ , etc.). A program, `ATMOSPHERE_PROFILE`, was created to perform a natural cubic spline interpolation of the FASCODE tropical atmosphere profile. This interpolates the profile to either the default layer boundaries or boundaries specified by the user. These quantities are stored in a file for use with the `MAKE_ATMOSPHERE` program. The program accepts a base pressure and temperature and then calculates the pressures at the layer boundaries using equation 3.5 and the boundary temperatures using equation 3.18. Above an altitude of 12 km, the ozone layer begins to affect the temperature and pressure of the layers. At this point the program uses the splined values from the FASCODE tropical atmosphere profile. The `MAKE_ATMOSPHERE` program performs the Curtis Godson approximation from equation 3.8 to find equivalent pressures for the layers. Using equation 3.7, the average molecular densities for the layers are calculated. Average mixing ratios from the FASCODE profile are used with equation 3.22 to find the layer column abundances for each molecular species. The temperature at the layer boundaries below 12 km is found using equation 3.18 and the mean layer equivalent temperatures are found using equation 3.19. The equivalent values for pressure, temperature, densities, and column abundances are stored in a file for inspection and for use by `ULTRAM`.

After the model atmosphere has been defined, the main radiative transfer modelling routine begins. The main model program, called `ULTRAM`, begins by loading in the atmosphere files produced by `MAKE_ATMOSPHERE`. It also loads the spectral line data

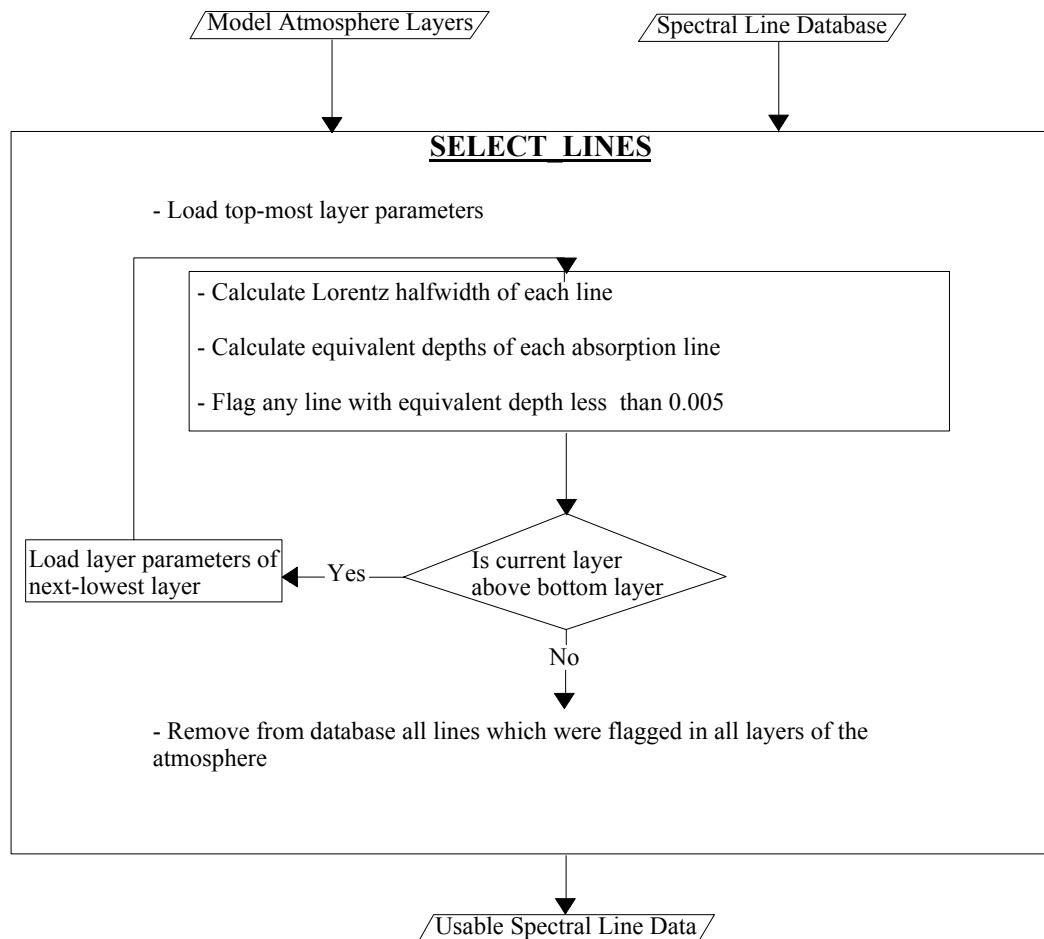


Figure 3.9: Flowchart of the `SELECT_LINES` function, which selects spectral lines of high enough intensity to include in the radiative transfer calculation.

from a file produced earlier from the Hitran database [16]. Using the function `MOLECULAR_LINES`, all relevant line data is loaded into a variable for use with the model. This line data is used by the function `SELECT_LINES` which selects only lines above a certain intensity threshold to optimize the radiative transfer computation.

The function `SELECT_LINES`, shown in the flowchart in figure 3.9, makes use

of the weak approximation of the *integrated absorptance* (equation 2.41) of an absorption line to determine if it should be included in the modelling run, increasing the efficiency of ULTRAM by removing lines too weak to be seen. Starting with the top layer of the atmosphere, the layer parameters are loaded in to the function. The function calculates the Lorentz half-width of each spectral line using equation 2.35 and uses this to calculate the equivalent depth of the absorption line using the weak approximation from equation 2.41. An arbitrary depth limit is set at 0.005. Any spectral lines with depths less than 0.005 (equivalent to 0.5% absorption) for the layer are flagged. This process is repeated for each layer, moving downwards to ground level, and any spectral lines which were flagged for all of the layers are removed from the spectral line database. This reduced line database is passed back to the main program for use in the radiative transfer calculations.

The main program begins the radiative transfer modelling by passing the spectral line data, atmospheric profile, and molecular abundance data to the LAYERS function, shown in the flowchart in figure 3.10. This function calculates either the transmittance or radiance at the given wavenumber using the radiative transfer method. LAYERS is the *engine* of the program that does the line-by-line, layer-by-layer calculations. The function begins by selecting the spectral lines whose line centers are within  $25 \text{ cm}^{-1}$  of the current wavenumber since lines outside this range have negligible contributions to the absorption coefficient,  $k_{\sigma}$ . In the case of ozone lines with their much narrower Doppler profile, only spectral lines within  $1 \text{ cm}^{-1}$  of the current wavenumber are accepted, further increasing the efficiency of the computation.

After the lines relevant to the calculation have been selected, the function loads

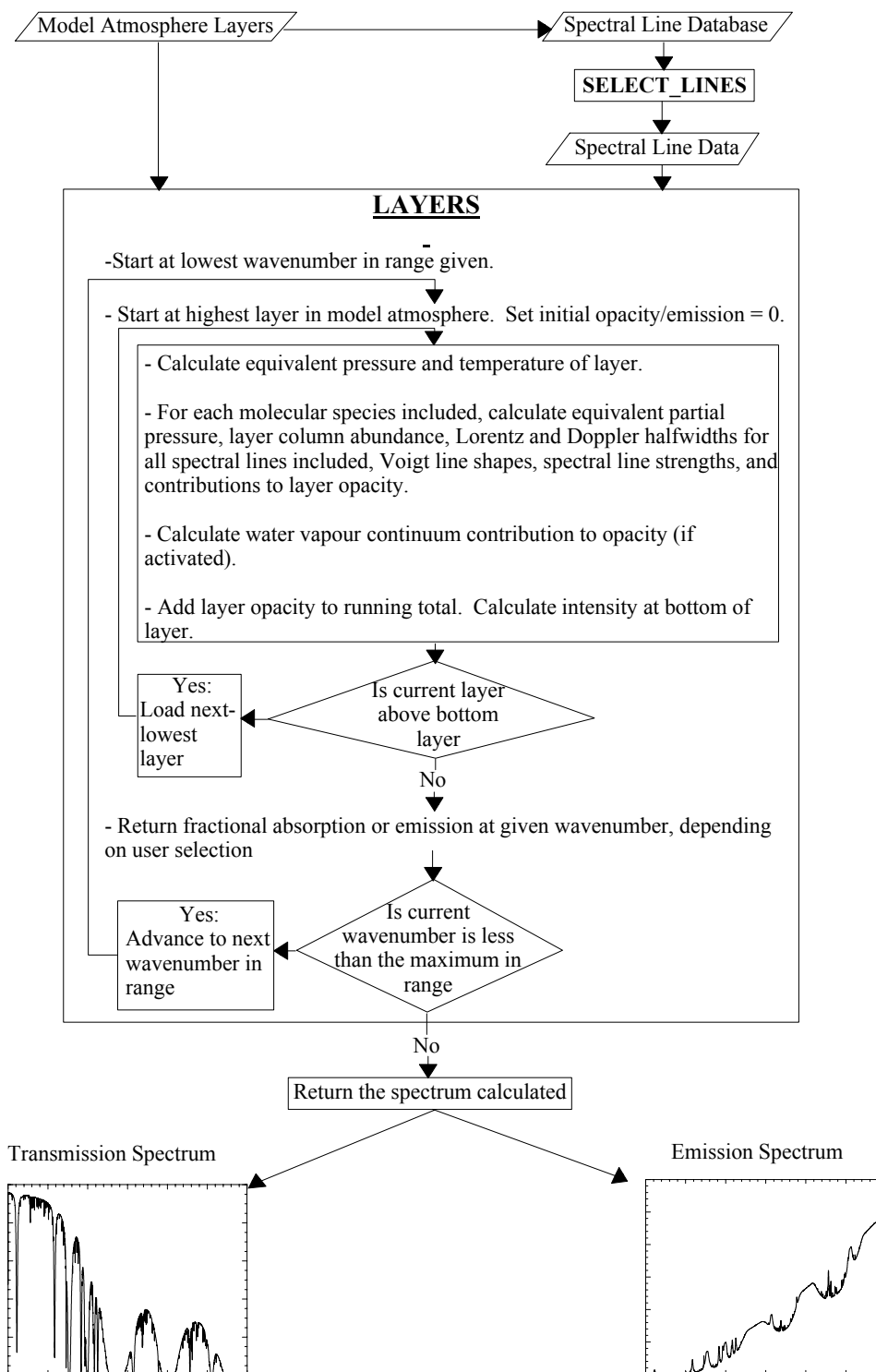


Figure 3.10: Flowchart of the LAYERS function, the main engine of ULTRAM.

the parameters for the top layer of the atmosphere. The function calculates the partial pressure of each species using equation 3.26. Next, the Doppler widths and Lorentz half-widths of all the lines are calculated using equations 2.33 and 2.35 respectively. Then, the values of the line shapes at the given wavenumber are calculated using the Voigt line shape function which is based on equation 3.27. The water vapour spectral line shapes are modified by subtracting the pedestal function given in equations 3.31 and 3.32. The spectral line strength values at the given wavenumber are calculated using equation 2.38. Finally, the contribution of each line to an overall opacity is calculated using equation ?? with equations 3.23 and 2.27. After the opacity contributions of all spectral lines have been calculated, they are summed to give an overall opacity at the current wavenumber due to spectral lines for the layer.

The next step is to calculate the contribution of the water vapour continuum if it is to be included. First, the partial pressure of water vapour and of the remainder of the atmosphere are calculated. Next, the self-continuum coefficient is corrected for the layer temperature. The total opacity contribution of the water vapour continuum for the layer is then calculated using equation 3.34.

The total opacity of the line is then calculated as the sum of the line opacity and the continuum opacity. The opacity for the layer is then added to a running total of the opacity. If the model is set to return radiance, this total opacity is used in equation 2.22 to calculate the intensity of radiation exiting the bottom of the layer. The radiance at the top of the atmosphere is taken to be zero. The algorithm repeats the process for each layer of the atmosphere, moving down one layer at a time.

If the model is set to return radiance, the LAYERS function calculates the intensity exiting from the bottom layer of the atmosphere. If the model is set to give transmittance, the LAYERS function returns the total opacity at the bottom of the atmosphere. The LAYERS function returns to the main program the radiance or transmittance for each sample point in the spectrum. At this stage it is customary to convolve the spectrum with the instrument line shape (ILS) function of a spectrometer, simulating an actual measurement. This allows the user to produce a spectrum that one would expect to observe with a specific spectrometer. In the present case, the spectrum was convolved with a Gaussian ILS having a full-width at half-max of  $0.005 \text{ cm}^{-1}$ . Other common ILS' such as triangle, sinc, or sinc-squared are also available.

### 3.5.3 ULTRAM Results

As was mentioned in § 3.3.3, this thesis is concerned with two main spectral regions: the SCUBA submillimeter range from  $5 \text{ cm}^{-1}$  to  $35 \text{ cm}^{-1}$  and the IRMA mid-infrared range from  $475 \text{ cm}^{-1}$  to  $575 \text{ cm}^{-1}$ . Each of these spectral regions must be modelled accurately in order to obtain a clear understanding of the correlations between water vapour measurements with IRMA and SCUBA. Table 3.2 highlights several parameters involved in modelling each spectral region.

It was considered important as a first step to ensure that ULTRAM gave the same results as FASCODE under the same conditions. Both ULTRAM and FASCODE allow the user to select the output to be returned in terms of transmittance (between 0 and 1)

	Submillimeter	MIR
Range ( $\text{cm}^{-1}$ )	5 – 35	475 – 575
Resolution ( $\text{cm}^{-1}$ )	0.001	0.001
Layers	31	31
H <sub>2</sub> O Lines	299	551
O <sub>3</sub> Lines	2237	120
O <sub>2</sub> Lines	243	0
CO <sub>2</sub> Lines	0	2107
Total Lines	2779	2778
Time (s)	738	1790

Table 3.2: Radiative transfer modelling parameters for the submillimeter and mid-infrared regions.

or in terms of radiance ( $\text{W m}^{-2} \text{sr}^{-1} \text{cm}^{-1}$ ). Astronomers are usually interested in transmittance data because it reveals wavelength ranges which are ‘windows’ for observations of astronomical objects. Radiance data are more appropriate for applications which involve remotely sensing molecular abundances in the atmosphere. Each of these output selections (transmission or radiance) can be returned by ULTRAM as either a spectrum for a given precipitable water vapour amount or as a three-dimensional data cube with varying precipitable water vapour amounts.

One difference between the models is that FASCODE used the 1986 version of the Hitran molecular line database [27] while ULTRAM used the 2000 version of the Hitran database [18]. This latest version of the Hitran database has updated values for spectral line strengths and half-widths. In particular, one of the improvements is the inclusion of self broadening values. A comparison of spectra obtained using the two databases with the same atmospheric layers will show some subtle differences due to updates in the spectral line parameters.

For the comparison with FASCODE, 1 mm pwv was chosen as the standard column

abundance of water vapour. Since FASCODE is not easily changed, ULTRAM used the same atmospheric layers as those produced by running the FASCODE auto-layering routine. Both models were run with identical layer parameters (i.e. pressures, temperatures, molecular densities, layer boundaries).

Figure 3.11 shows the submillimeter transmission spectra as produced by FASCODE (black) and ULTRAM (red). The ULTRAM spectrum is displaced vertically for clarity. The top panel in the figure shows the entire submillimeter range. Two submillimeter windows can be seen: one from  $20\text{ cm}^{-1}$  to  $24\text{ cm}^{-1}$  (known as the  $450\text{ }\mu\text{m}$  window) and another from  $26\text{ cm}^{-1}$  to  $30\text{ cm}^{-1}$  (known as the  $350\text{ }\mu\text{m}$  window). The middle panel shows an expanded view of the  $450\text{ }\mu\text{m}$  window. A strong water vapour line can be seen centered on  $20.7\text{ cm}^{-1}$  and an oxygen line can be seen at about  $23.85\text{ cm}^{-1}$ . The shallow, narrow spectral lines across the top of each spectrum are a manifold of ozone lines. The bottom panel shows a further expansion of the complex manifold of spectral lines. Spectral lines of water vapour, ozone, and oxygen are present in this region. The spectra are seen to be in excellent agreement.

The mid-infrared transmission spectrum is shown in figure 3.12. Again, the ULTRAM spectrum (red) is shifted vertically from the FASCODE spectrum (black) for clarity. The top panel shows the IRMA range from  $500\text{ cm}^{-1}$  to  $550\text{ cm}^{-1}$ . This spectral range includes numerous water vapour lines and carbon dioxide lines. The middle panel is an expanded view of one of the windows in this region. It shows several water vapour lines (such as the one at about  $534.25\text{ cm}^{-1}$ ). A close inspection of this panel shows subtle differences in the lines produced by FASCODE and ULTRAM. For example, the water vapour line at

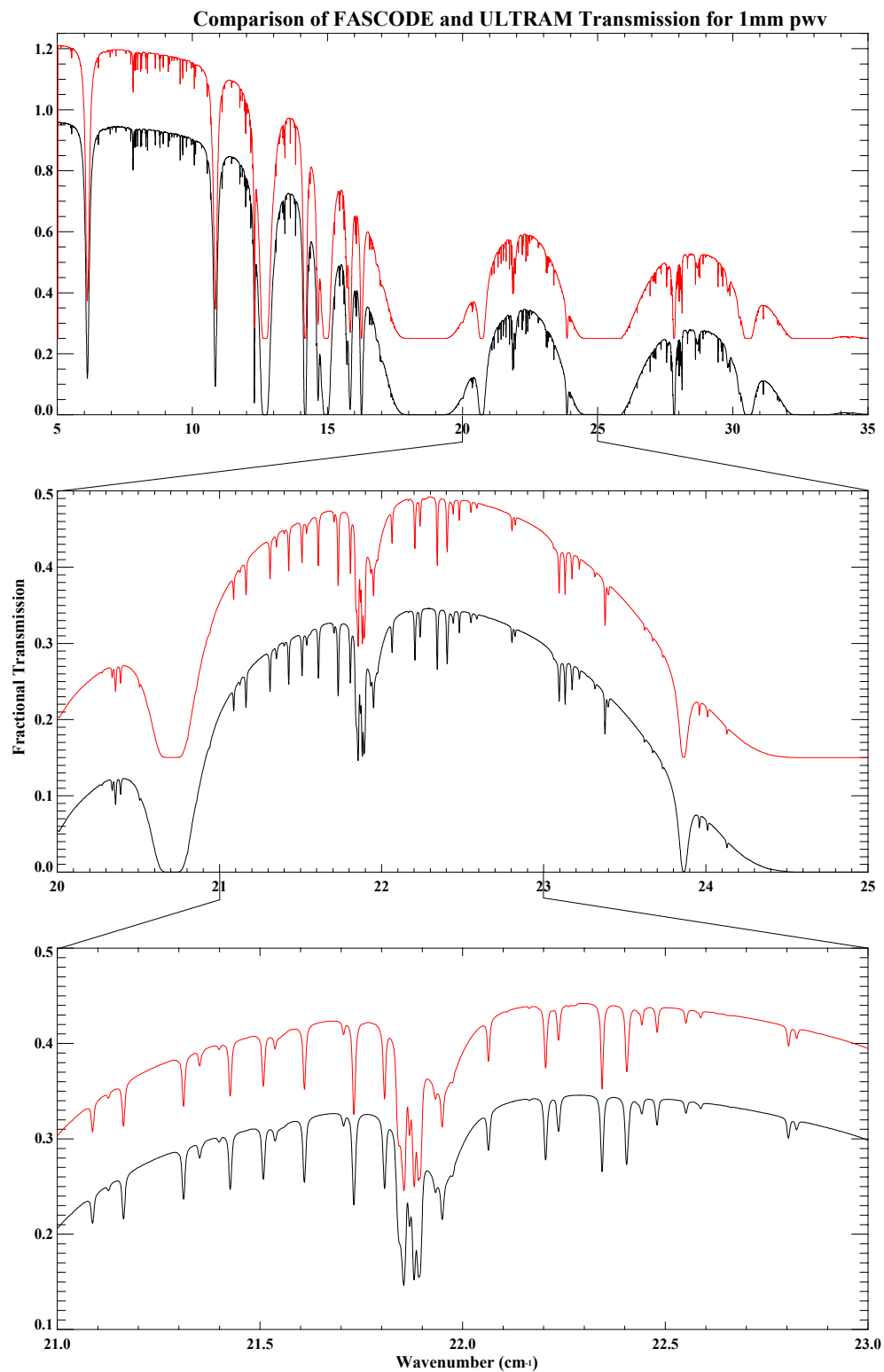


Figure 3.11: Comparison of simulated (sub)millimeter transmission spectra for 1 mm pwv from ULTRAM (red) and FASCODE (black).

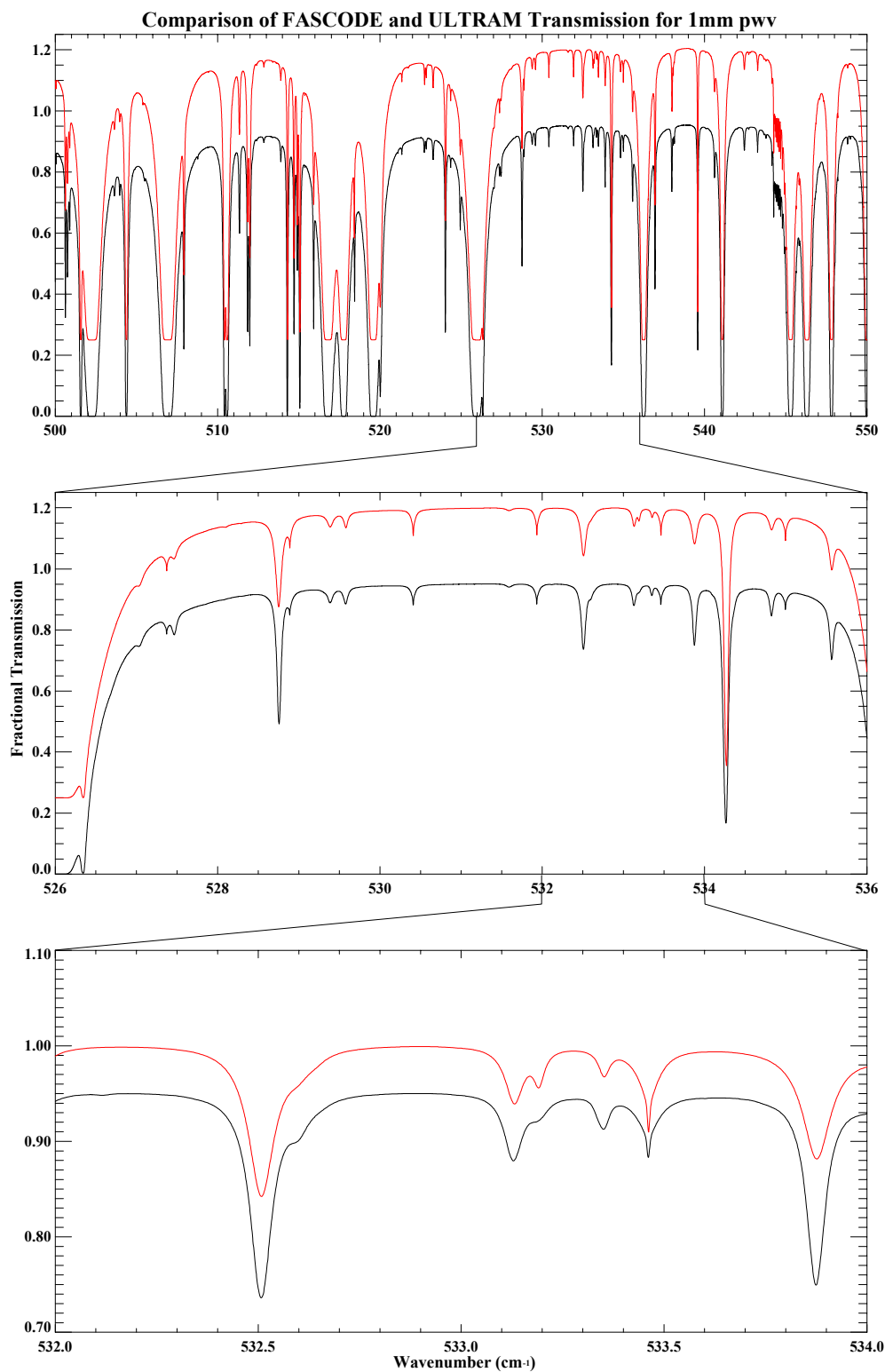


Figure 3.12: Comparison of simulated mid-infrared transmission spectra for 1 mm pwv from ULTRAM (red) and FASCODE (black).

about  $528.75 \text{ cm}^{-1}$  appears weaker in the ULTRAM output than in the FASCODE output. This is due to an adjustment of the line parameters in the updated Hitran spectral line database. The bottom panel of the figure shows a further expansion of a portion of the window. Again, the spectral lines in the ULTRAM output are subtly different from the FASCODE output due to updates in the line parameters in the newer database. Despite the changes in the spectral line database, ULTRAM shows a high level of agreement with FASCODE in this spectral region.

Figure 3.13 compares the submillimeter emission spectra from ULTRAM and FASCODE. The ULTRAM spectrum (red) is again vertically displaced above the FASCODE spectrum (black) for clarity. The top panel of the figure shows the entire submillimeter region and is populated with spectral lines of water vapour, oxygen, and ozone. The middle panel shows an expanded view of the  $450 \mu\text{m}$  window with a strong water vapour line at about  $21.7 \text{ cm}^{-1}$ , an oxygen line at about  $23.85 \text{ cm}^{-1}$ , and a manifold of weak ozone lines between them. The bottom panel is a further expanded view of this window, focusing on the complex region between  $21.8 \text{ cm}^{-1}$  and  $22.1 \text{ cm}^{-1}$ . The models show a high level of agreement in this spectral region.

Figure 3.14 shows the comparison of mid-infrared emission spectra. Good agreement between the models is seen and differences in the line parameters are evident in this figure. An important difference between the spectra in these two regions is in the baseline slopes of the spectra. The slope in the submillimeter region is due to the slope of the Rayleigh-Jeans tail of the Planck function. The mid-infrared region has a smaller slope because the Planck function is near its peak at these wavenumbers.

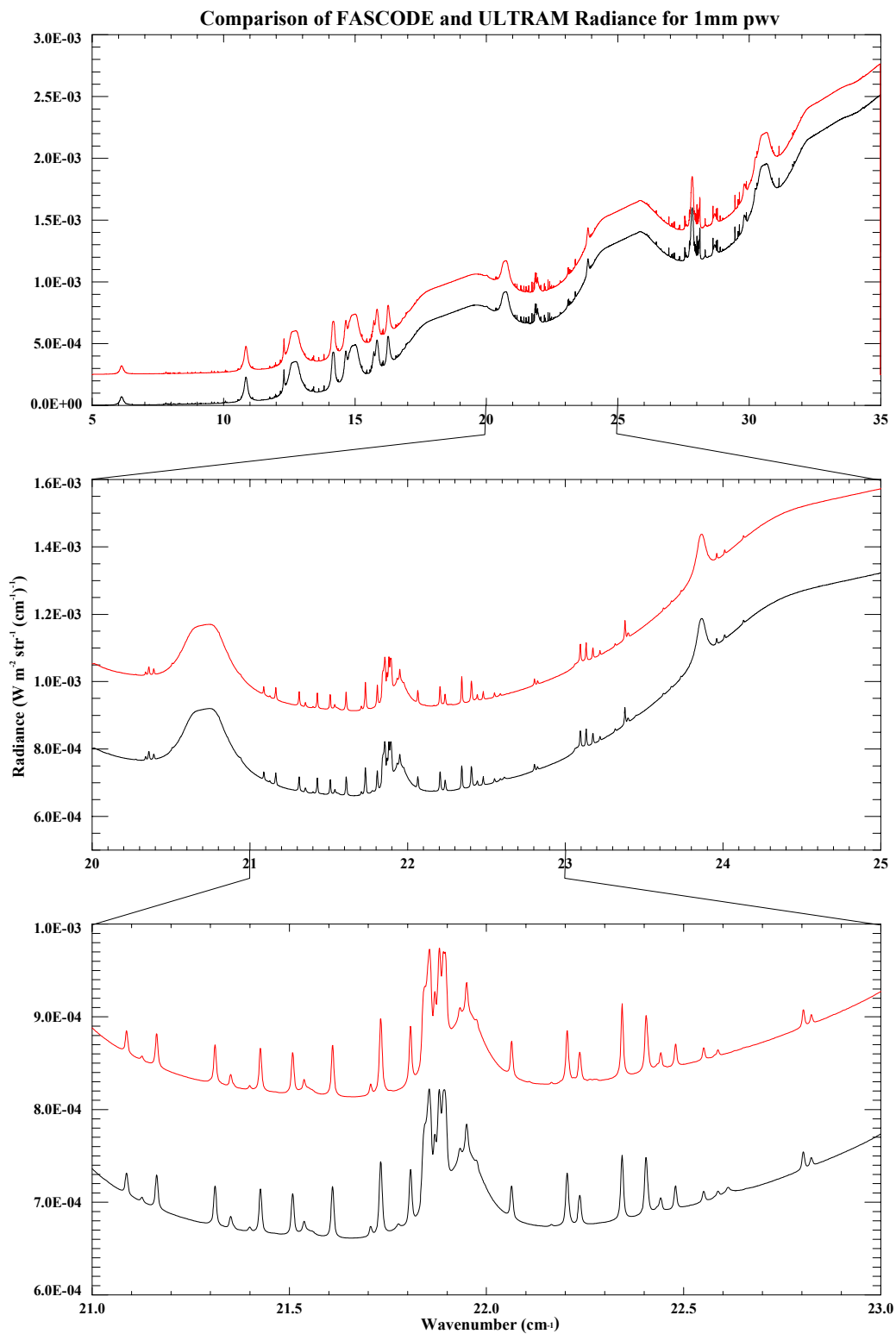


Figure 3.13: Comparison of simulated (sub)millimeter radiance spectra for 1 mm pwv from ULTRAM (red) and FASCODE (black).

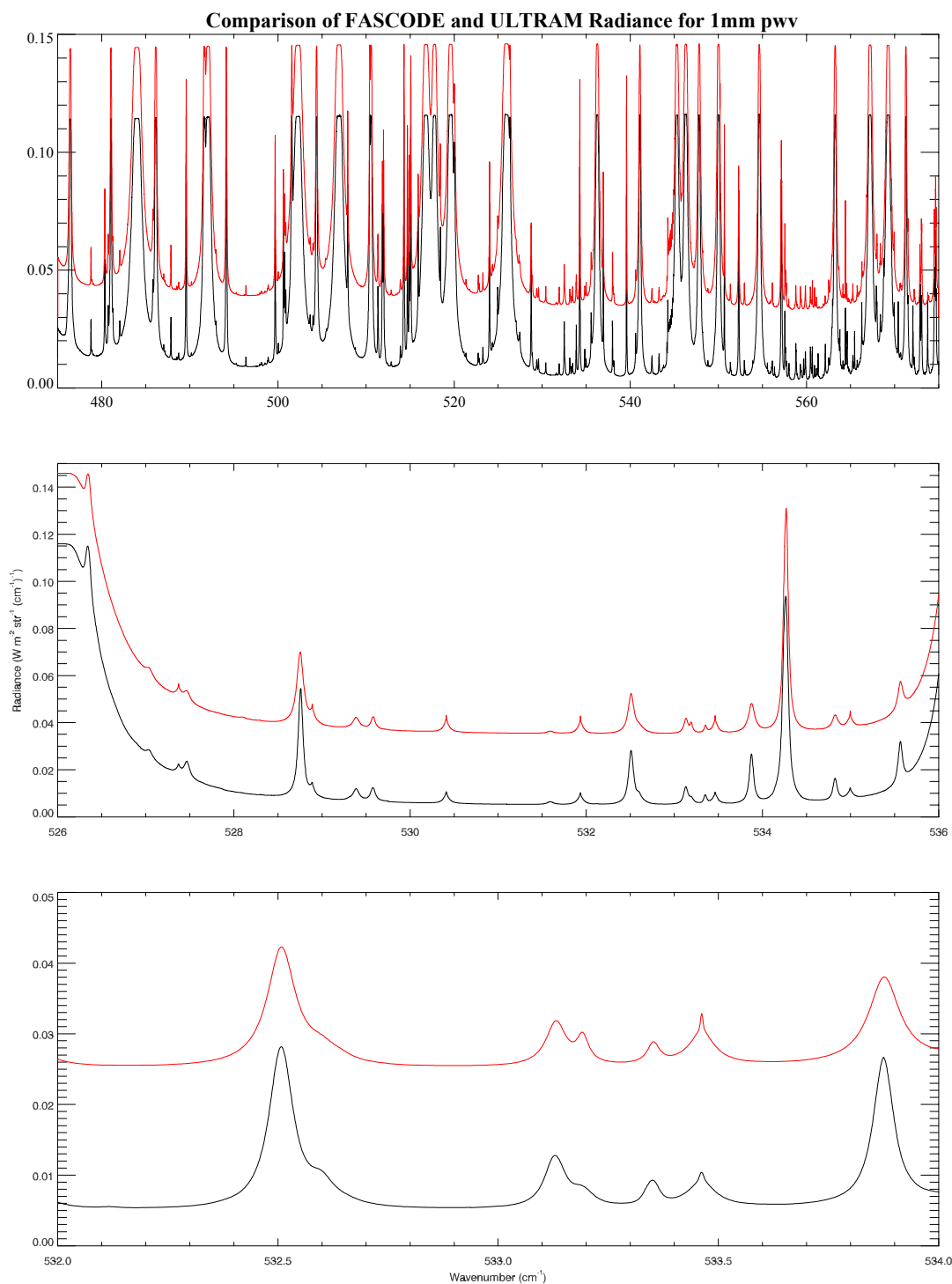


Figure 3.14: A comparison of the simulated mid-infrared radiance spectra produced by ULTRAM (red) and FASCODE (black).

Since ULTRAM has been shown capable of replicating the FASCODE output, it can be used to model spectra at submillimeter and mid-infrared wavelengths. Using ULTRAM, it is possible to investigate the effects of changing the pressure, temperature, and molecular abundance profiles of the atmosphere. To construct a data cube, ULTRAM is run several times, increasing the precipitable water vapour amount by 0.1 mm each time. The resulting data set, covering a range of 0.1 - 2.0 mm pwv, can be plotted in 3 dimensions (wavenumber, transmission or emission, mm pwv), to show the evolution of the spectra with changing water vapour amounts. The data cube forms a comprehensive database which can be used to study radiometer bands under different atmospheric conditions.

ULTRAM has been shown to accurately reproduce results from FASCODE calculations. Because of its flexibility, ULTRAM can be used to investigate theoretically the correlation between measurements of the radiance of water vapour at submillimeter and mid-infrared wavelengths. This investigation provides an independent theoretical basis for a comparison with the results obtained with IRMA II and SCUBA on Mauna Kea as presented in chapter 5.